

See discussions, stats, and author profiles for this publication at: <https://www.researchgate.net/publication/264269037>

Dynamic Doping in Planar Ionic Transition Metal Complex-Based Light-Emitting Electrochemical Cells

ARTICLE in ADVANCED FUNCTIONAL MATERIALS · JULY 2013

Impact Factor: 11.81 · DOI: 10.1002/adfm.201202689

CITATIONS

17

READS

37

8 AUTHORS, INCLUDING:



[Stephan van Reenen](#)

Technische Universiteit Eindhoven

14 PUBLICATIONS 220 CITATIONS

[SEE PROFILE](#)



[David Hartmann](#)

11 PUBLICATIONS 260 CITATIONS

[SEE PROFILE](#)



[Henk J. Bolink](#)

University of Valencia

208 PUBLICATIONS 4,871 CITATIONS

[SEE PROFILE](#)



[A. Winnacker](#)

Friedrich-Alexander-University of Erlangen-...

298 PUBLICATIONS 3,725 CITATIONS

[SEE PROFILE](#)

Dynamic Doping in Planar Ionic Transition Metal Complex-Based Light-Emitting Electrochemical Cells

Sebastian B. Meier, Stephan van Reenen, Bastien Lefevre, David Hartmann, Henk J. Bolink, Albrecht Winnacker, Wiebke Sarfert,* and Martijn Kemerink*

Using a planar electrode geometry, the operational mechanism of iridium(III) ionic transition metal complex (iTMC)-based light-emitting electrochemical cells (LECs) is studied by a combination of fluorescence microscopy and scanning Kelvin probe microscopy (SKPM). Applying a bias to the LECs leads to the quenching of the photoluminescence (PL) in between the electrodes and to a sharp drop of the electrostatic potential in the middle of the device, far away from the contacts. The results shed light on the operational mechanism of iTMC-LECs and demonstrate that these devices work essentially the same as LECs based on conjugated polymers do, i.e., according to an electrochemical doping mechanism. Moreover, with proceeding operation time the potential drop shifts towards the cathode coincident with the onset of light emission. During prolonged operation the emission zone and the potential drop both migrate towards the anode. This event is accompanied by a continuous quenching of the PL in two distinct regions separated by the emission line.

1. Introduction

Solid-state light-emitting electrochemical cells (LECs)^[1–3] are one of the latest classes of organic light sources and have generated great interest during recent years. LECs are single-layer solution-processable electroluminescent devices comprising a luminescent material in an ionic environment.^[4–10] Due to their peculiar operational mechanism, LECs allow for charge

carrier injection from air-stable electrodes and low operating voltages, consequently giving rise to high power efficiencies.^[11,12] These advantages make LECs a promising candidate for cost-efficient next generation solid-state lighting and signage applications. However, in comparison to multi-layer organic light-emitting diodes, their state-of-the-art performances such as lifetimes, power efficiencies and achievable colors are significantly poorer. To further enhance the performances of LECs it is necessary to improve the understanding of their peculiar operation mechanisms.

Two different kinds of LECs can be distinguished on the basis of the nature of the luminescent material. Devices based on an emissive conjugated polymer admixed with a salt and a solid electrolyte are termed polymer LECs (pLECs),^[1,2,9,10] whereas LECs comprising an ionic transi-

tion metal complex (iTMC) lead to iTMC-LECs.^[3–8] The latter in general do not require an electrolyte as the emitting species is intrinsically ionic. Nonetheless, ionic liquid (IL) is frequently added, especially in the case of iridium(III)-based devices, to accelerate their turn-on.^[13] iTMCs dissolve in benign solvents allowing for environmentally friendly processing. In addition, higher efficiencies can be expected due to the phosphorescent nature of the transition metal complexes.^[14,15] Another benefit arises from the ease of color tunability in iridium(III) ionic transition metal complexes (Ir-iTMCs) which enables an available color range covering the entire visible spectrum, including white.^[7,8,16–20] Recently iTMC-LECs have been achieved with simultaneous sub-second turn-on and long lifetime (>4000 h) at high brightness (>600 cd m⁻²), demonstrating their potential as alternative light sources.^[21]

The operational mechanism of LECs has been the subject of an intense debate^[22–24] ever since their invention by Pei et al. in 1995.^[1] Two competing models have been proposed, the electrodynamic model (ED)^[25–28] and the electrochemical doping model (ECD),^[1,2,29–32] and measurement results have been interpreted in either of them. The underlying physics of both models can be best described by considering the predicted steady-state operation of LECs as illustrated in Figure 1. The ED states that nearly all applied potential drops at the two electrode interfaces owing to the formation of very thin layers of accumulated and uncompensated ions (Figure 1a). On the one hand these electric double layers (EDLs) enhance charge carrier

S. B. Meier, Prof. A. Winnacker
Department of Materials Science VI: Materials
for Electronics and Energy Technology
Friedrich-Alexander University of Erlangen-Nuremberg
Martensstr. 7, 91058 Erlangen, Germany

S. B. Meier, B. Lefevre, Dr. D. Hartmann, Dr. W. Sarfert
Siemens AG, Corporate Technology
CT RTC MAT MPV-DE, Günther-Scharowsky-Str. 1,
91058 Erlangen, Germany
E-mail: wiebke.sarfert@siemens.com

S. van Reenen, Dr. M. Kemerink
Department of Applied Physics
Eindhoven University of Technology
PO Box 513, 5600 MB, Eindhoven, The Netherlands
E-mail: m.kemerink@tue.nl

Dr. H. J. Bolink
Instituto de Ciencia Molecular
Universidad de Valencia
Catedrático José Beltrán 2, 46980 Paterna, Spain

DOI: 10.1002/adfm.201202689



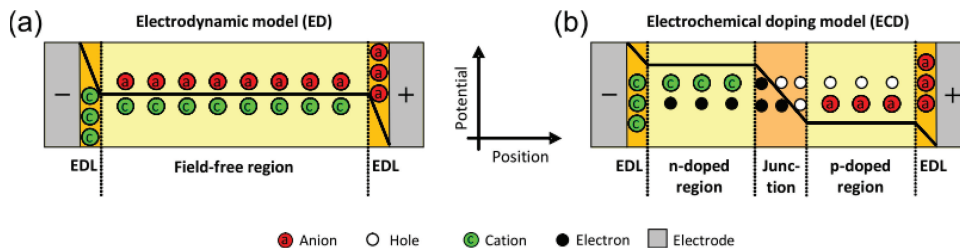


Figure 1. Schematic illustration of a) the electrodynamic model (ED) and b) the electrochemical doping model (ECD) during steady-state describing the operational mechanism of light-emitting electrochemical cells. The bold black line represents the electrostatic potential profile in between the electrodes whereas the ionic and electronic charge distributions are labeled according to the legend. High- and low-field regions are highlighted in orange and light yellow color, respectively.

injection from the electrodes and on the other hand they screen the bulk active layer from the external electrical field, necessitating a diffusion-driven electronic current. In the ECD (Figure 1b) charge accumulation and EDL formation at the electrodes are assumed as well, however, the most important aspect here is the oxidation and reduction of the luminescent material by injected electrons and holes from the electrode contacts. These redox processes are accompanied by the movement of cations and anions to the redox centers to stabilize and electrostatically compensate the injected charge carriers resulting in an electrochemical doping process similar to the static situation in doped inorganic semiconductors. The doping gives rise to highly conductive p- and n-doped zones adjacent to the electrodes with enhanced carrier density and mobility.^[33] Due to ion depletion^[29] a narrow intrinsic region arises in between the doped zones where the remainder of the applied potential drops and electron/hole recombination takes place to cause light-emission. In the ECD both drift and diffusion contribute to charge carrier transport.^[34]

Confirmation of both models was initially done in planar electrode configuration with inter-electrode spacings ranging from the μm - to the cm-scale by scanning Kelvin probe microscopy (SKPM) and optical experiments using predominantly polymer LECs. Utilizing these methods, features of both the ECD and the ED have been observed in pLECs.^[30–32,35–37] Recently, their appearance was found to depend on the injection properties of the contacts.^[34] In the case that EDL formation leads to ohmic contacts the ECD is observed. In the commonly used sandwiched device configuration, in which the electrode spacing is much smaller (typically in the range of 200 nm), the ECD was proven by current characterization techniques like impedance spectroscopy.^[38,39] Such a broad variety of experimental evidence is not available for small molecular iTMC-LECs. Until now planar iTMC-LECs were only reported to operate according to the ED.^[28] Additionally, few works exist describing experimental results in sandwiched configuration which support the ECD.^[21,40–43] Hence, there still remains doubt concerning the operation mechanism of iTMC-LECs which is hindering its further progress.

Here, we report the results of transient experiments carried out on planar iTMC-LECs using as active material the ionic iridium(III) complex bis-2-phenylpyridine 6-phenyl-2,2'-bipyridine iridium(III) hexafluorophosphate [$\text{Ir}(\text{ppy})_2(\text{pbpy})$] $[\text{PF}_6]$ admixed with the ionic liquid 1-butyl-3-methylimidazolium hexafluorophosphate [BMIM] $[\text{PF}_6]$. A combination of

fluorescence and optical microscopy was used to probe the photoluminescent behavior of the iTMC in between the planar electrodes during operation and after switch-off and to identify the location of the emission zone. SKPM was performed to record the evolution of the electrostatic potential. The outcomes of both studies, PL quenching during operation and a sharp potential drop far away from the electrodes, are in line with each other and confirm that iTMC-based LEC devices, just as their polymer counterparts, work according to an electrochemical doping mechanism.

2. Results and Discussion

The chemical structures of the compounds used and a sketch of the investigated planar device architecture are depicted in Figure 2a. Details about the device preparation can be found in the Experimental section. Two sets of indium tin oxide (ITO) interdigitated electrodes (IDEs) with different electrode spacings of 5 μm and 10 μm were used. A section of a bright field optical microscopy picture of the 10 μm gap electrode structure is depicted in Figure 2b. The energy level diagram of the device is shown in Figure 2c.

2.1. Fluorescence Microscopy

First analyses were performed using an IDE device with an inter-electrode spacing of 10 μm . Even though IL was admixed to the iTMC to accelerate the device response,^[13] a high voltage of 210 V was used to operate the LEC. This will be commented on in the second section of this article but we note that also without additional IL added the iTMC-LEC does work at 210 V. As expected the time scales are, however, dramatically slowed down by roughly two orders of magnitude. To study the photoluminescent behavior of iTMC-LECs during device operation, fluorescence microscopy was carried out under near-UV illumination of the active layer. Additionally images of the plain electroluminescence without photo-excitation were recorded to be able to identify the location of the emission zone within the inter-electrode spacing. Details concerning the experimental setup and procedure can be found in the Experimental Section. Microscopy images were taken of a section of the cell, highlighted in Figure 2b, at different time intervals during operation of the LEC both with and without UV illumination

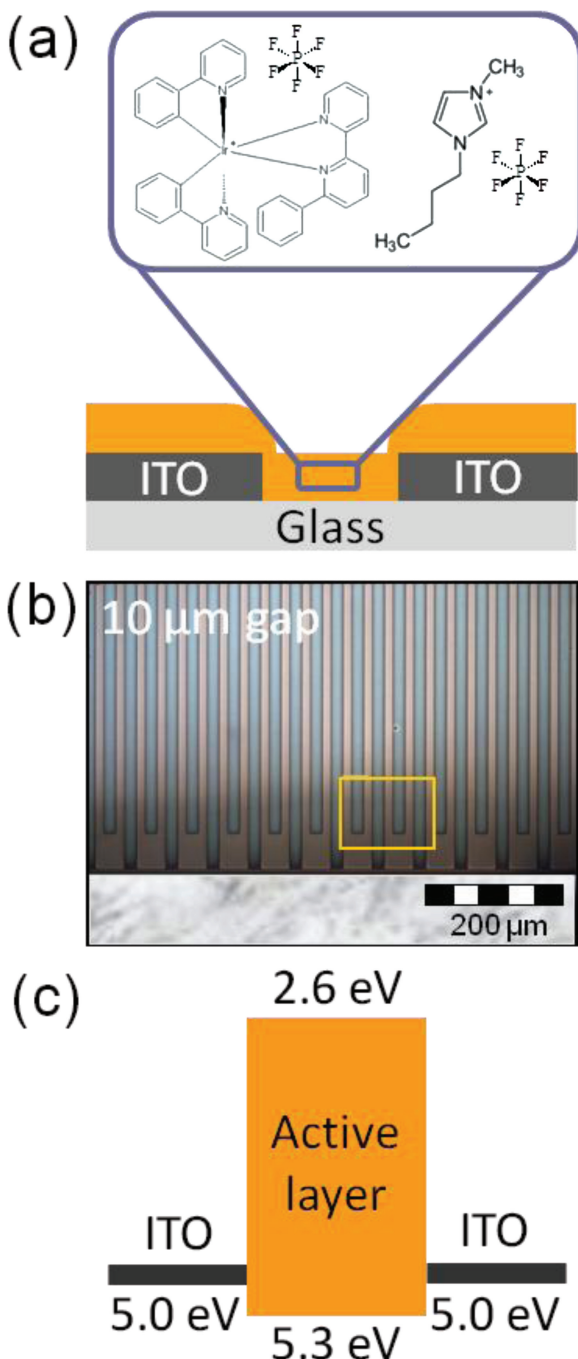


Figure 2. a) Schematic device layout and structural formulae of the organic constituents. b) Optical microscopy image of a 10 μm interdigitated electrode structure. The yellow frame reflects the picture section of the images in Figure 3. c) Energy level diagram of the planar LEC device.

(Figure 3). To facilitate the evaluation we superimposed the fluorescence image with the plain EL image so that both the fluorescence and the electroluminescence can be observed. As pre-patterned IDE substrates were used, the active layer covered also the finger-like electrodes, referred to as bottom or buried electrode configuration, for which reason the whole device area

revealed UV excited PL. Moreover, the dark spots that appear in the image of the pristine (undriven) device (Figure 3a) are due to particles in the UV light source. With a new lamp the spots did not appear any longer (Figure 3f).

The current flowing through the entire interdigitated electrode device was also monitored during the operation of the LEC. From the logarithmic presentation (Figure 4) three different regimes can be easily identified. Initially, during the first 15 min of operation, the current increases linearly which is associated with quenching of the PL in the inter-electrode gap (Figure 3a,b). Intuitively one would relate this decrease in PL to the degradation of the iTMC. However, as we will demonstrate below, this is not what is predominantly happening during device operation. After 15 min of driving a positive change in the current slope is observed. This change coincides with the onset of weak light emission, visible as the orange line in Figure 3c. For clarity, the image in Figure 3c does not exactly correspond to the beginning of the light emission but to a marginally later point in time (18 min). This is due to the fact that the light intensity immediately after the onset of emission is very weak and can not be distinguished in the recorded image. However, by using image processing software to adjust the brightness and contrast settings of the image, light emission can be visualized and identified to be located very close to the cathode interface after 15 min of operation (see Supporting Information Figure S1,S2). Moreover, the emission line clearly separates two distinct regions within the inter-electrode spacing of which the major region adjacent to the anode shows more pronounced PL quenching compared to the thinner region adjacent to the cathode. During the second regime, up to 100 minutes, the emission line moves towards the middle of the interelectrode gap and becomes brighter (Figure 3c,d). Furthermore, the PL quenching in the two regions next to the emission line becomes more intense, still being more pronounced in the region adjacent to the anode. In the third regime, after 100 minutes of operation, the current density reaches a plateau until the end of the measurement after 1000 min. During this time interval the emission line migrates slowly further towards the anode and the light intensity decreases (Figure 3d,e). The PL quenching in both the anodic and cathodic region is strong and is approximately equal in magnitude. The fact that quenching is also observed on top of the cathode (Figure 3c,e) will be discussed later on. After turning off the bias and allowing the device to relax for nearly 1000 h it was studied again under UV illumination (Figure 3f). Compared to the condition immediately before switch-off (Figure 3e) an almost entire recovery of the PL intensity in between the electrodes and atop the cathode is observed. This relaxation process occurred slowly over the duration of several hours.

In view of the previous observations, planar iTMC-LECs possess clear features in accordance with the ECD.^[1,2,30–32] As both p- and n-type doping quench the photo-excited PL, doped regions appear darker than undoped regions.^[30,31,36,37,44] The quenching of the PL during operation can therefore be attributed to electrochemical doping of the iTMC layer in between the electrodes, p-type at the anode and n-type at the cathode, which finally gives rise to a light emitting p-i-n junction. The p-doping process can be envisioned as the trapping of injected holes on the iridium iTMC cation stabilized by uncompensated

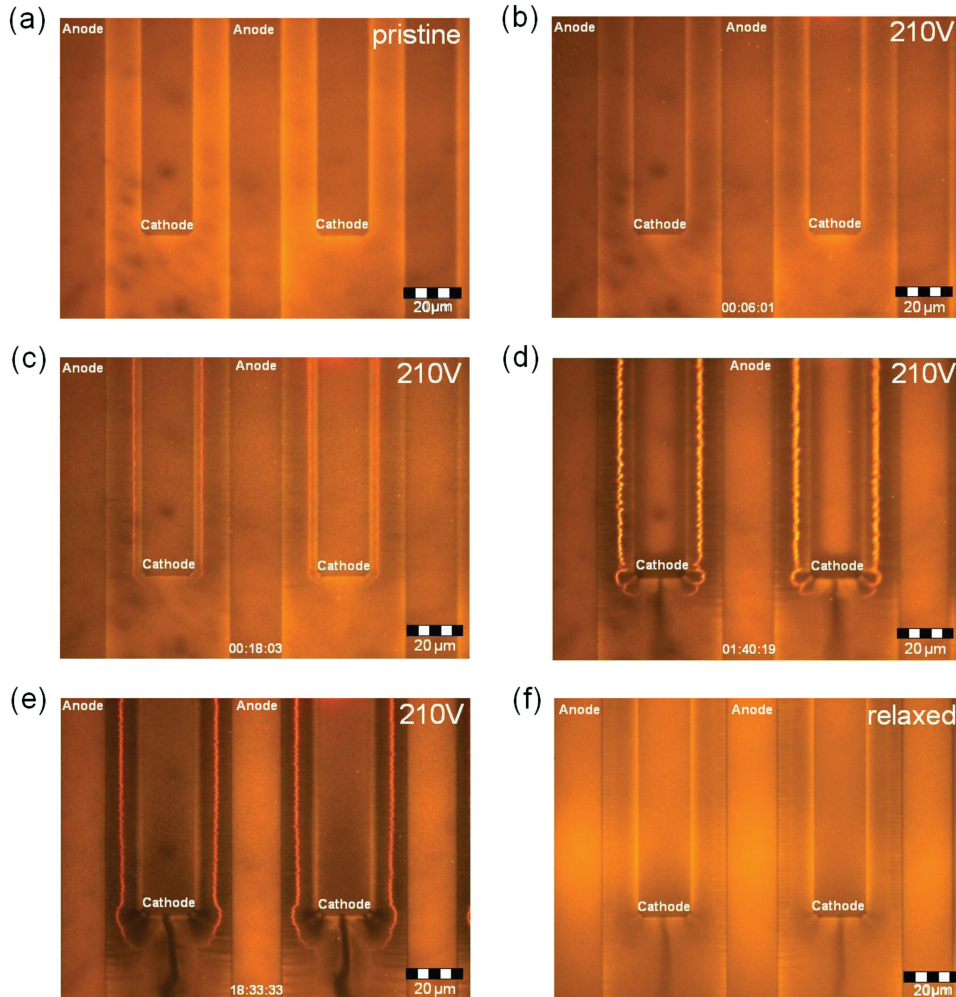


Figure 3. Fluorescence microscopy investigation of a planar iTMC-LEC with an inter-electrode spacing of $10\text{ }\mu\text{m}$ at various points in time during operation. A driving voltage of 210 V was applied. a) UV image of the pristine device. b–e) Superimposed UV illuminated and optical images at various points in time during operation. f) UV image of a driven device after relaxation for 1000 h .

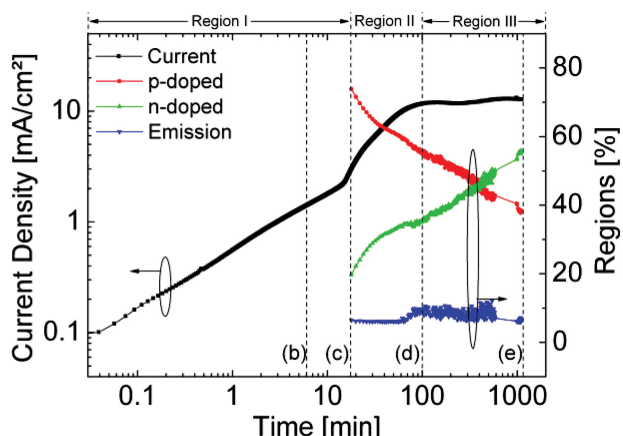


Figure 4. Transient current and evolution of the dimensions of the p-doped region, the n-doped region and the emission zone of a planar iTMC-LEC with an inter-electrode spacing of $10\text{ }\mu\text{m}$ at a driving voltage of 210 V . The percentage of the doped regions and the emission zone refer to the total inter-electrode area.

PF_6^- anions. In case of n-doping the iTMC cation itself acts as the counter charge for the injected electrons. The quenching almost entirely disappears after turning off the bias which may be related to either dedoping of the iTMCs or to diffusion of electrochemically damaged iTMC cations out of the imaging zone. The latter might be possible as the active material was not only restricted to the inter-electrode spacing but instead covered the whole device area.

To probe a possible diffusivity of the bulky iridium cations we performed a fluorescence recovery after photobleaching (FRAP) experiment (see Experimental Section for details). The outcomes of the study are illustrated in Figure 5. Figure 5a,b reveal a pristine iTMC-LEC photobleached for 24 h and the same device 39 h after the bleaching was stopped, respectively. During the chosen recovery period neither significant changes in the dimensions of the bleaching spot nor differences in its coloring could be observed. In contrast, as depicted in Figure 5c,d, respectively, a LEC electrically driven for 24 h at 210 V shows a clearly diminished quenching intensity in the inter-electrode area after a recovery period of 39 h , in conjunction with the

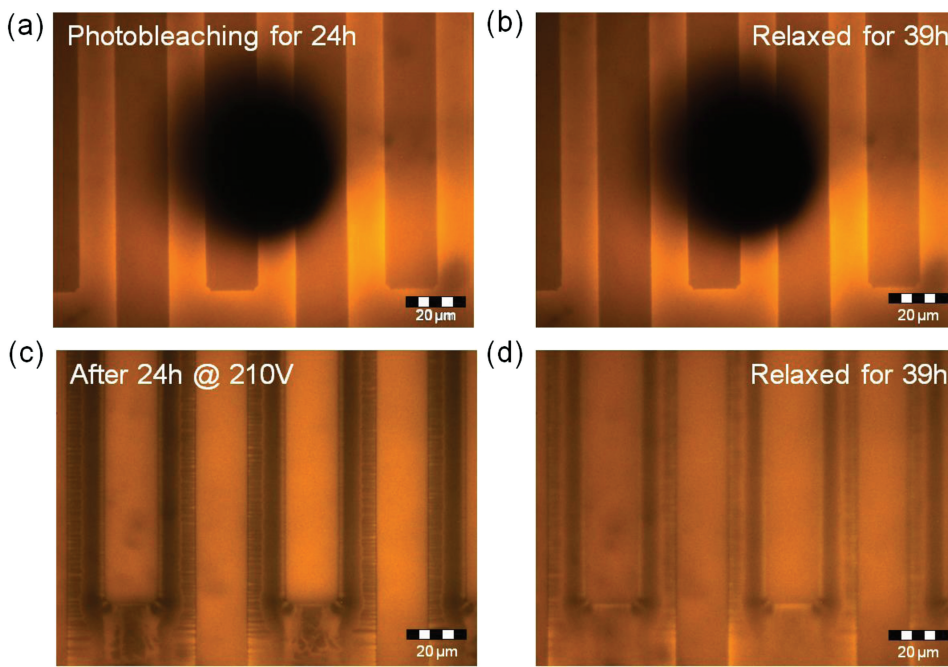


Figure 5. a) Planar iTMC-LEC after 24 h of local photobleaching with near-UV light. b) Same device as in (a) after a recovery period of 39 h after the photobleaching was stopped. c) Planar iTMC-LEC after 24 h of operation at 210 V. d) Same device as in (c) after a recovery period of 39 h after bias switch-off.

results demonstrated before (Figure 3e,f). From the experiment we can conclude that on the one hand the iTMC cation is not or only marginally mobile and on the other hand that the PL recovery of the electrically operated LEC is due to the dedoping of the iTMCs. The PL quenching is nearly completely reversible after an extended recovery period (Figure 3f) indicating that virtually no permanent degradation occurred during the time frame of these analyses.

As the position of the narrow electroluminescent zone within the inter-electrode spacing is related to the dimensions of the p- and n-doped regions, their fractions with respect to the total inter-electrode area were calculated as a function of operation time by means of image processing (see Experimental Section for brief details) and the results are included in Figure 4. Note that the first calculations could not be run before the onset of clearly visible light emission after 18 min, as the emission line served as the border for the determination of the doped regions. Moreover, due to its jagged shape, the emission line captures a quite large fraction of the inter-electrode spacing of 5–10%. The outcomes of the calculations in Figure 4 clearly demonstrate a large extent of p-type doping (>70%) during the early stages of operation and only a small fraction of n-type doping (<20%). During the subsequent operation the p-doped region is gradually consumed by the n-doped region. A description of this process can be found in the literature.^[45] N-type doping becomes dominant after around 400 min and covers more than 55% of the entire inter-electrode area in the end of operation after 1000 min. The results are in accord with the emission line forming at the cathode and moving towards the anode and highlight the prerequisite for a migration of the emission zone in LECs: the consumption of one kind of doping by the other.

2.2. Scanning Kelvin Probe Microscopy

In addition to the PL experiments we performed scanning Kelvin probe microscopy (SKPM) to study the transient behavior of the electrostatic potential in the planar iTMC-LEC. The outcomes are plotted in Figure 6. Due to restrictions in the measurement setup the maximum voltage that could be applied to the LEC was limited to 100 V. As this voltage was not sufficient to observe light emission in a device with 10 μm inter-electrode spacing, we used IDEs with a smaller gap size of 5 μm for these investigations. This electrode spacing can also be clearly deduced from the height profile which is depicted in Figure 6a. For clarity the anode and cathode edges are labeled correspondingly. The height scan was recorded along the horizontal dashed blue line denoted in the AFM topography image which is displayed as the top inset in Figure 6a. This line also corresponds to the scan direction for the measurement of the potential profiles during operation which are also included in Figure 6a. The arrow denotes the temporal evolution of the electrostatic potential within a time interval of roughly 4.5 h. The reason not to use a 5 μm device as well for the fluorescence microscopy investigations in the previous section is that this would have led to substantial losses in the image resolution due to the smaller dimensions of the device structure.

The first SKPM measurement was performed immediately after applying a bias of 100 V to the iTMC-LEC at which a sharp potential drop is registered in the middle of the inter-electrode gap. During the subsequent 30 min of operation the potential drop shifts towards the cathodic interface whereas with prolonged operation it moves in the opposite direction and is displaced towards the anode by the end of the device operation.

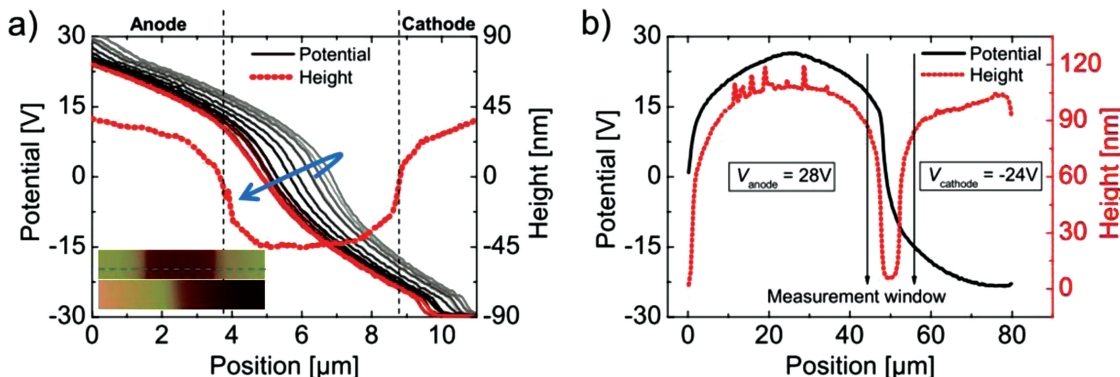


Figure 6. a) Height and transient potential profiles during operation of an iTMC-LEC. The inset shows AFM images of the topography (top) and the potential map (bottom). The dashed lines indicate the orientation of the profiles with respect to the electrodes and the arrow denotes the temporal evolution of the potential. b) Complete potential profile across the LEC biased at 52 V. The arrows indicate the measurement window of the profiles shown in (a).

For visualization purposes a topography and potential map recorded during the later stages of operation are shown in the bottom part of the inset in Figure 6a. The present findings are in full agreement with the ECD^[1,2,30–32] especially with regard to recent SKPM studies on planar pLECs^[32,34,46] and provide clear evidence for the formation of a p-i-n junction in iTMC-LECs. The ED which predicts potential drops to occur only at the electrode interfaces,^[25–28] can be ruled out. Our results demonstrate that during the entire SKPM analysis the potential drop occurs within the inter-electrode gap far away from the contacts. This implies the existence of a high-ohmic intrinsic region where the large electric field has to compensate for the low conductivity. Moreover, the intrinsic area is not fixed to a specific position in between the electrodes but migrates with time as visualized by the shift of the potential drop.

Even though devices with two different inter-electrode spacings have been used, the results of the SKPM and fluorescence microscopy study are in excellent agreement. The initially centered drop of the electrostatic potential implies that p- and n-doping set in immediately. Note that in the fluorescence microscopy experiments no EL could be detected in the first 15 min. This is probably related to a relatively low doping density. As the doping density continuously increases, the EL increases until at some moment it is large enough to be observed. The shift of the potential drop in the SKPM experiments is in accordance with the fluorescence investigations.

Such shifts may be related to imbalances in carrier injection, conductivity, doping speed or a combination of these. We note that even though a voltage of 100 V has been applied to operate the planar iTMC-LEC, a large portion of the potential is screened from the inter-electrode spacing and drops on top of the electrodes (Figure 6a). This screening as well as the PL quenching observed on top of the cathode (Figure 3d,e) indicates that doping also takes place atop the electrodes. The absence of quenching on top of the anode may be due to a difference in quenching cross-sections or doping density.

As the length of the previous potential scans was limited and did not involve the entire electrodes' width, we performed a larger-area scan in a separate SKPM measurement to record the complete potential profile across the LEC. To allow for

a stable SKPM measurement with reliable results, the maximum voltage that could be applied to the LEC was limited to below 60 V and we chose a voltage of 52 V. The outcome of the experiment is illustrated in Figure 6b, which, for comparison, also shows the measurement window for the recording of the potential profiles in the initial study. Again a large drop of the electrostatic potential is observed in the inter-electrode gap and also atop both electrodes. Moreover, the full applied potential is visible which separates into 28 V in the anodic region and -24 V in the cathodic region. A rough estimate of the potential drop in the inter-electrode gap yields a value of 25 V which implicates large potential drops of more than 10 V atop each electrode. The large potential screening from the gap may be related to the presence of EDLs that consume more potential than one would expect from the size of the injection barriers: 0.3 and 2.4 eV (Figure 2c). Indeed numerical simulations shown in the Supporting Information confirm the possibility of having such large EDLs in combination with doping, i.e., larger interfacial potential drops, and concomitantly larger fields, are needed to enable sufficient injection to match the bulk conductivity. In the simulations, the enhanced carrier injection on top of the electrodes also results in electrochemical doping. Experimentally this is observed as a quenching of the PL on top of the cathode (Figure 3d,e). This indicates that the geometry of the device may play a role in carrier transport and, related to this, in the positions of the doped regions as well as of the p-i-n junction. Apart from this no qualitative effects on the operating mechanism are expected which is confirmed by the 2D numerical simulations in the Supporting Information. Additionally the simulations document that the potential drop over the EDLs cannot be observed when buried electrodes are used, in accordance with our experimental findings (Figure 6). Using top electrodes instead, the existence of EDLs has already been experimentally confirmed in pLECs.^[34,46]

A remaining issue is the extremely large bias voltage of $\sim 100\text{ V}$ needed to operate the iTMC-LECs. Similar bias voltages have been used in pLECs with millimeter-sized gaps.^[30] Later the voltage was reduced by operation above the melting temperature of the electrolyte^[47] or by a different choice of electrolyte.^[48] The device physics was, however, not affected. In all

cases a thin recombination zone positioned in between two oppositely doped regions was observed. Here, the use of relatively large bias voltages was necessary to reduce the turn-on time as well as to obtain detectable light emission. The generally low turn-on time of iTMC-LECs in comparison to pLECs seems to be related to pronounced differences in the ionic conductivities, a topic which is addressed in a very recent publication.^[49]

Finally, based on the present findings and the literature results, a few differences can be distinguished between planar polymer and iTMC-LECs. First of all relatively large potential drops over the EDLs seem to be present in the Ir-iTMC LEC in contrast to pLECs where these drops equal the injection barriers.^[34,46] This may be related to the sensitivity of LEC operation on the electrode contacts as previously addressed. For example injection limitation was demonstrated to result in a device behavior according to the ED whereas the ECD holds when charge injection is non-limited.^[34] In general the electrode work function was shown to affect charge carrier injection and doping in LECs.^[36,50] Moreover, in the doped regions of iTMC-LECs large potential drops are identified (Figure 6), whereas in pLECs based on MDMO-PPV this is typically not the case.^[34] However, in LECs based on MEH-PPV relatively large electric fields are detected in the n-doped region.^[32,37] This indicates a compensation of dissimilarities between the carrier conductivity in the doped and undoped regions by the electric field distribution. A similarly large field seems to be needed in both doped regions in the iTMC-LEC (Figure 6a), which spans a gap of 5 µm. Hence, these devices still deviate from the idealized LEC in that they are still sensitive to the inter-electrode distance and, related to that, are too resistive to be operated at relatively low bias voltages. The operational mechanism, however, remains the same: electrochemical doping enables enhanced carrier injection and transport, while the applied field redistributes to maximize the overall current passing through.

3. Conclusions

By a combination of fluorescence and scanning Kelvin probe microscopy insight is gained in the operational mechanism of planar ionic transition metal complex-based light-emitting electrochemical cells. Quenching of the photoluminescence in the inter-electrode gap and a sharp drop in the electrostatic potential far away from the electrodes confirm an electrochemical doping mechanism which results in the formation of a light-emitting p-i-n junction. The intrinsic region, where light emission occurs, is not fixed but migrates with time which might be related to a change in the conductivity of electrons and holes. The results provide a fundamental basis for a better understanding of iTMC-based LEC devices and additionally demonstrate an important challenge: an emission zone centered and fixated in the middle of the inter-electrode spacing immediately at the beginning of operation to allow for stable and efficient light-emission.

4. Experimental Section

Device Preparation: Bis-2-phenylpyridine 6-phenyl-2,2'-bipyridine iridium(III) hexafluorophosphate $[\text{Ir}(\text{ppy})_2(\text{bpyp})]\text{PF}_6$ was synthesized

similarly according to methods described previously.^[51,52] Acetonitrile (anhydrous, 99.8%) and the ionic liquid (IL) 1-butyl-3-methylimidazolium hexafluorophosphate [BMIM][PF₆] (purum, ≥97.0%) were obtained from Sigma Aldrich and used as-received. Indium tin oxide (ITO)-coated glass substrates (ShinAn SNP) were photolithographically structured to yield ITO interdigitated electrodes (IDEs) with spacings of 5 µm and 10 µm. The ITO electrodes had a height of 100 nm and were contacted via evaporated chromium supplies. Before use the substrates were extensively cleaned using sonication in detergent bath and distilled water as well as subsequent oxygen plasma treatment. The latter improved the wettability of the emitter solution on the substrate and additionally resulted in an increase of the ITO work function^[53] giving rise to better alignment to the HOMO level of the iridium complex. A stock solution was prepared, dissolving five percent by weight of the iridium complex and the IL in a molar ratio of 3:1 in Acetonitrile. IL was used to decrease the turn-on time of the devices.^[13] The stock solution was filtered using a 0.1 µm PTFE-filter and spin-coated on top of the IDE substrates (750 rpm, 60 s) under ambient conditions. Afterwards the substrate was transferred to an argon filled glovebox (O₂ and H₂O <1 ppm) and annealed on a hotplate at 100 °C for 1 h to give a final active layer thickness of 100 nm as determined by a KLA Tencor P-15 profilometer. To test the devices under ambient conditions they were encapsulated under inert atmosphere by a cavity glass capping (Shanghai Amerina Optoelectronic) equipped with a silica getter to protect the active layer against penetrating oxygen and water. The capping was directly glued to the substrate without prior removal of the organic layers using a self-made, two-component, Bisphenol A-based, UV-curable epoxy adhesive which was coated locally onto the margin of the capping. To test the functionality of the encapsulation, control devices were processed using a calcium layer as a sensor. As the calcium sensor stayed metallic during the long-term study of several hundreds of hours, a possible reaction with water and oxygen to CaO or Ca(OH)₂, which would have changed the optical appearance and the resistivity of the transparent film, could be excluded.

Fluorescence Microscopy: Images of the optically excited photoluminescence of the iTMC-LECs were recorded with an Olympus BX61 microscope equipped with a fluorescence unit which consists of a high pressure mercury vapor arc discharge lamp and a super wide band mirror (SWBM). The SWBM comprised an excitation filter, a dichromatic mirror and an emission filter. Emitted light from the mercury lamp was reduced to the spectral range in between 380 nm and 400 nm via the excitation filter and was then reflected by the dichromatic mirror to impinge on the planar LEC device. The photoexcited light of the LEC passed through the dichromatic mirror and the emission filter and was collected by the microscopy optics. To decrease the intensity of the incident light on the sample in order to avoid photoinduced degradation and to be able to observe the weak electroluminescence, two additional grey filters were used. Images of the device without photoexcitation were taken as well to identify the location of the emission zone. Interdigitated electrodes (IDEs) with a gap size of 10 µm were used and a voltage of 210 V was applied to the device to study the transient evolution of the photoluminescence and electroluminescence during a period of roughly 18 h. Images were recorded every 60 s with an exposure time of 7 s. In parallel with the optical probing, the current was measured with a computer-controlled source-measure unit (Keithley 2400). The measurements were performed at room temperature.

Image Processing: To calculate the proportions of the p- and n-doped region as well as of the emission zone of the entire inter-electrode area, image processing was performed on every single picture recorded during the fluorescence microscopy study. As the emission line served as the border for the determination of both regions the first calculations could not be run before the onset of clearly visible light emission. In brief, the images were initially converted to grayscale and then transferred to binary values (bright regions = 1 and dark regions = 0). The bright (emissive) and two dark (doped) regions are purged from background noise and finally the proportions of each region are calculated by relating the number of pixels in each region to the total amount of pixels in the image.

Fluorescence Recovery After Photobleaching (FRAP): The FRAP experiment was carried out by using the emitted and spectrally reduced light of the mercury lamp of the Olympus BX61 microscope (see fluorescence microscopy paragraph). To allow for maximum near-UV light intensity on the LEC in order to effectively photobleach the iTMCs no grey filters were used. Bleaching was performed for 24 h with a subsequent recovery period of 39 h. Images were recorded every 60 s with an exposure time of 7 s. The measurements were performed at room temperature.

Scanning Kelvin Probe Microscopy (SKPM): SKPM images were recorded in a glove box under N_2 atmosphere ($[O_2] < 1$ ppm and $[H_2O] < 1$ ppm) with a Veeco Instruments MultiMode AFM with Nanoscope IV controller, operating in lift mode with a lift height of 50 nm. Ti-Pt coated silicon tips (MikroMasch NSC36/Ti-Pt, $k \sim 1.75$ N m $^{-1}$) were employed. IDEs with a gap size of 5 μ m were used and a voltage of 100 V was applied to the device to study the transient evolution of the electrostatic potential during a period of roughly 4.5 h. The measurements were carried out at room temperature.

Supporting Information

Supporting Information is available from the Wiley Online Library or from the author.

Acknowledgements

S.B.M., B.L., D.H., W.S., and H.B. acknowledge financial support from the European Community's Seventh Framework Program under grant agreement n° FP7-ICT-248043 (CELLO-project.eu). S.v.R. and M.K. acknowledge financial support from the Dutch program NanoNextNL.

Received: September 17, 2012

Revised: December 4, 2012

Published online: February 26, 2013

- [1] Q. B. Pei, G. Yu, C. Zhang, Y. Yang, A. J. Heeger, *Science* **1995**, *269*, 1086.
- [2] Q. Pei, Y. Yang, G. Yu, C. Zhang, A. J. Heeger, *J. Am. Chem. Soc.* **1996**, *118*, 3922.
- [3] J.-K. Lee, D. S. Yoo, E. S. Handy, M. F. Rubner, *Appl. Phys. Lett.* **1996**, *69*, 1686.
- [4] J. D. Slinker, D. Bernards, P. L. Houston, H. D. Abruña, S. Bernhard, G. G. Malliaras, *Chem. Commun.* **2003**, *19*, 2392.
- [5] J. D. Slinker, J. Rivnay, J. S. Moskowitz, J. B. Parker, S. Bernhard, H. D. Abruña, G. G. Malliaras, *J. Mater. Chem.* **2007**, *17*, 2976.
- [6] F. Durum, D. Bertin, D. Gigmes, *Int. J. Nanotechnol.* **2012**, *9*, 377.
- [7] T. Hu, L. He, L. Duan, Y. Qiu, *J. Mater. Chem.* **2012**, *22*, 4206.
- [8] R. D. Costa, E. Ortí, H. J. Bolink, F. Monti, G. Accorsi, N. Armaroli, *Angew. Chem. Int. Ed.* **2012**, *51*, 8178.
- [9] L. Edman, *Electrochim. Acta* **2005**, *50*, 3878.
- [10] Q. Sun, Y. Li, Q. Pei, *J. Display Technol.* **2007**, *3*, 211.
- [11] H.-C. Su, C.-C. Wu, F.-C. Fang, K.-T. Wong, *Appl. Phys. Lett.* **2006**, *89*, 261118.
- [12] H. J. Bolink, E. Coronado, R. D. Costa, N. Lardiés, E. Ortí, *Inorg. Chem.* **2008**, *47*, 9149.
- [13] S. T. Parker, Jason D. Slinker, Michael S. Lowry, Marshall P. Cox, Stefan Bernhard, George G. Malliaras, *Chem. Mater.* **2005**, *17*, 3187.
- [14] H. Yersin, *Top. Curr. Chem.* **2004**, *241*, 1.
- [15] H. Yersin, A. F. Rausch, R. Czerwieniec, T. Hofbeck, T. Fischer, *Coord. Chem. Rev.* **2011**, *255*, 2622.
- [16] A. B. Tamayo, S. Garon, T. Sajoto, P. I. Djurovich, I. M. Tsypa, R. Bau, M. E. Thompson, *Inorg. Chem.* **2005**, *44*, 8723.
- [17] L. He, J. Qiao, L. Duan, G. Dong, D. Zhang, L. Wang, Y. Qiu, *Adv. Funct. Mater.* **2009**, *19*, 2950.
- [18] F. Kessler, R. D. Costa, D. Di Censo, R. Scopelliti, E. Ortí, H. J. Bolink, S. Meier, W. Sarfert, M. Grätzel, Md. K. Nazeeruddin, E. Baranoff, *Dalton Trans.* **2012**, *41*, 180.
- [19] H.-C. Su, H.-F. Chen, F.-C. Fang, C.-C. Liu, C.-C. Wu, K.-T. Wong, Y.-H. Liu, S.-M. Peng, *J. Am. Chem. Soc.* **2008**, *130*, 3413.
- [20] L. He, L. Duan, J. Qiao, G. Dong, L. Wang, Y. Qiu, *Chem. Mater.* **2010**, *22*, 3535.
- [21] D. Tordera, S. Meier, M. Lenes, R. D. Costa, E. Ortí, W. Sarfert, H. J. Bolink, *Adv. Mater.* **2012**, *24*, 897.
- [22] J. C. deMello, *Nat. Mater.* **2007**, *6*, 796.
- [23] Q. Pei, A. J. Heeger, *Nat. Mater.* **2008**, *7*, 167.
- [24] G. G. Malliaras, J. D. Slinker, J. A. DeFranco, M. J. Jaquith, W. R. Silveira, Y.-W. Zhong, J. M. Moran-Mirabal, H. G. Craighead, H. D. Abruña, J. A. Marohn, *Nat. Mater.* **2008**, *7*, 168.
- [25] J. C. deMello, N. Tessler, S. C. Graham, R. H. Friend, *Phys. Rev. B* **1998**, *57*, 12951.
- [26] J. C. deMello, J. J. M. Halls, S. C. Graham, N. Tessler, R. H. Friend, *Phys. Rev. Lett.* **2000**, *85*, 421.
- [27] J. C. deMello, *Phys. Rev. B* **2002**, *66*, 235210.
- [28] J. D. Slinker, J. A. DeFranco, M. J. Jaquith, W. R. Silveira, Y.-W. Zhong, J. M. Moran-Mirabal, H. G. Craighead, H. D. Abruña, J. A. Marohn, G. G. Malliaras, *Nat. Mater.* **2007**, *6*, 894.
- [29] D. L. Smith, *J. Appl. Phys.* **1997**, *81*, 2869.
- [30] J. Gao, J. Dane, *Appl. Phys. Lett.* **2003**, *83*, 3027.
- [31] J. Gao, J. Dane, *Appl. Phys. Lett.* **2004**, *84*, 2778.
- [32] P. Matyba, K. Maturova, M. Kemerink, N. D. Robinson, L. Edman, *Nat. Mater.* **2009**, *8*, 672.
- [33] S. van Reenen, R. A. J. Janssen, M. Kemerink, *Org. Electron.* **2011**, *12*, 1746.
- [34] S. van Reenen, P. Matyba, A. Dzwilewski, R. A. J. Janssen, L. Edman, M. Kemerink, *J. Am. Chem. Soc.* **2010**, *132*, 13776.
- [35] L. S. C. Pingree, D. B. Rodovsky, D. C. Coffey, G. P. Bartholomew, D. S. Ginger, *J. Am. Chem. Soc.* **2007**, *129*, 15903.
- [36] D. B. Rodovsky, O. G. Reid, L. S. C. Pingree, D. S. Ginger, *ACS Nano* **2010**, *4*, 2673.
- [37] Y. Hu, J. Gao, *J. Am. Chem. Soc.* **2011**, *133*, 2227.
- [38] A. Munar, A. Sandström, S. Tang, L. Edman, *Adv. Funct. Mater.* **2012**, *22*, 1511.
- [39] S. van Reenen, R. A. J. Janssen, M. Kemerink, *Adv. Funct. Mater.* **2012**, *22*, 4547.
- [40] M. Buda, G. Kalyuzhny, A. J. Bard, *J. Am. Chem. Soc.* **2002**, *124*, 6090.
- [41] H. Rudmann, S. Shimada, M. F. Rubner, *J. Appl. Phys.* **2003**, *94*, 115.
- [42] M. Lenes, G. Garcia-Belmonte, D. Tordera, A. Pertegás, J. Bisquert, H. J. Bolink, *Adv. Funct. Mater.* **2011**, *21*, 1581.
- [43] S. B. Meier, D. Hartmann, D. Tordera, H. J. Bolink, A. Winnacker, W. Sarfert, *Phys. Chem. Chem. Phys.* **2012**, *14*, 10886.
- [44] Y. Hu, C. Tracy, J. Gao, *Appl. Phys. Lett.* **2006**, *88*, 123507.
- [45] N. D. Robinson, J. Fang, P. Matyba, L. Edman, *Phys. Rev. B* **2008**, *78*, 245202.
- [46] S. van Reenen, P. Matyba, A. Dzwilewski, R. A. J. Janssen, L. Edman, M. Kemerink, *Adv. Funct. Mater.* **2011**, *21*, 1795.
- [47] J.-H. Shin, A. Dzwilewski, A. Iwasiewicz, S. Xiao, Å. Fransson, G. N. Ankah, L. Edman, *Appl. Phys. Lett.* **2006**, *89*, 013509.
- [48] J.-H. Shin, L. Edman, *J. Am. Chem. Soc.* **2006**, *128*, 15568.
- [49] S. van Reenen, T. Akatsuka, D. Tordera, M. Kemerink, H. J. Bolink, *J. Am. Chem. Soc.* **2013**, *135*, 886.
- [50] D. Hohertz, J. Gao, *Adv. Mater.* **2008**, *20*, 3298.
- [51] H. J. Bolink, E. Coronado, R. D. Costa, E. Ortí, M. Sessolo, S. Gruber, K. Doyle, M. Neuburger, C. E. Housecroft, E. C. Constable, *Adv. Mater.* **2008**, *20*, 3910.
- [52] F. Gärtner, D. Cozzula, S. Losse, A. Boddien, G. Anilkumar, H. Junge, T. Schulz, N. Marquet, A. Spannenberg, S. Gladiali, M. Beller, *Chem. Eur. J.* **2011**, *17*, 6998.
- [53] D. Milliron, I. Hill, C. Shen, J. Kahn, A. Schwartz, *J. Appl. Phys.* **2000**, *87*, 572.